

# Laboratory-Based Maximum Slip Rates in Earthquake Rupture Zones and Radiated Energy

by A. McGarr, J. B. Fletcher, M. Boettcher, N. Beeler, and J. Boatwright

**Abstract** Laboratory stick-slip friction experiments indicate that peak slip rates increase with the stresses loading the fault to cause rupture. If this applies also to earthquake fault zones, then the analysis of rupture processes is simplified inasmuch as the slip rates depend only on the local yield stress and are independent of factors specific to a particular event, including the distribution of slip in space and time. We test this hypothesis by first using it to develop an expression for radiated energy that depends primarily on the seismic moment and the maximum slip rate. From laboratory results, the maximum slip rate for any crustal earthquake, as well as various stress parameters including the yield stress, can be determined based on its seismic moment and the maximum slip within its rupture zone. After finding that our new equation for radiated energy works well for laboratory stick-slip friction experiments, we used it to estimate radiated energies for five earthquakes with magnitudes near 2 that were induced in a deep gold mine, an  $M$  2.1 repeating earthquake near the San Andreas Fault Observatory at Depth (SAFOD) site and seven major earthquakes in California and found good agreement with energies estimated independently from spectra of local and regional ground-motion data. Estimates of yield stress for the earthquakes in our study range from 12 MPa to 122 MPa with a median of 64 MPa. The lowest value was estimated for the 2004  $M$  6 Parkfield, California, earthquake whereas the nearby  $M$  2.1 repeating earthquake, as recorded in the SAFOD pilot hole, showed a more typical yield stress of 64 MPa.

## Introduction

Ever since [Brace and Byerlee \(1966\)](#) suggested that stick-slip friction events in the laboratory are useful analogs for understanding earthquakes, there have been numerous studies intended to bridge the gap between friction experiments and natural earthquakes. In this study, we attempt to bridge this gap by first reviewing laboratory evidence that maximum slip rates can be related to the yield strength of the laboratory fault. We then proceed to our main objective of testing the hypothesis that slip rates in the rupture zones of earthquakes depend on the local yield strength and are independent of factors that may vary from one earthquake to another, such as the distribution of slip.

To this end, we develop an equation for estimating energy radiation that is consistent with our hypothesis. This equation depends mostly on the seismic moment and the maximum slip rate within the high-slip region of the earthquake rupture zone. As we will show, radiated energies estimated independently from ground-motion spectra agree with those calculated using our new approach, suggesting that our hypothesis is realistic.

The maximum slip rates needed to estimate radiated energy, as well as various stress parameters, including yield

stress, can be inferred by analytically matching a laboratory stick-slip friction experiment to an earthquake based on its seismic moment and maximum slip ([McGarr \*et al.\*, 2009](#)). As will be seen, for the earthquakes investigated in this study, our inferred maximum slip rates are mostly in the range 2–8 m/s, in agreement with rates estimated in a previous study ([McGarr and Fletcher, 2007](#)) that was based on a different method using earthquake slip models.

The yield stresses, inferred from this same analysis, are distributed about a median value of 64 MPa, which is consistent with the deepest *in situ* stress measurements, as we will show. Interestingly, our lowest yield stress was inferred for the  $M$  6 2004 Parkfield earthquake, about 12 MPa, which is consistent with other indicators of low strength for the San Andreas fault in this region ([Hickman and Zoback, 2004](#); [Williams \*et al.\*, 2004](#)).

## Maximum Slip Rates in the Laboratory

Laboratory friction experiments involving precut faults (e.g., [Dieterich, 1981](#)) are well suited to exploring the effect of fault-zone strength on the peak slip rate. To do this, we use

the results of 15 biaxial friction experiments (Table 1) reported by Lockner and Okubo (1983) and one result from a triaxial experiment at much higher loading stresses (Koizumi *et al.*, 2004) to assess the relationship between yield stress,  $\tau_1$ , and the maximum slip rate  $\dot{D}_{\max}$ .

The biaxial experiments were performed on a large granite sample with a pre-cut fault that is 2 m long and 0.4 m wide. The strength of the fault can be controlled by adjusting the normal stress acting on the fault surface. As is typical for crustal rocks, fault strength is linear with normal stress (e.g., Byerlee, 1968). Experimentally, dynamic rupture commences when the applied shear stress reaches the yield stress  $\tau_1$  (Fig. 1). Johnson and Scholz (1976) demonstrated that for this type of experiment, the rise time  $T$  for slip to increase from zero to its final value is controlled by the unloading stiffness and mass of the experimental set-up but is independent of the loading stresses (Lockner and Okubo, 1983; Beeler, 2006). In the case of the experiments reported by Lockner and Okubo (1983),  $T$  is always close to 2 ms, as seen in Figure 1a (bottom trace).

Because the traces of slip rate during a stick-slip event are quite noisy (Fig. 1a, middle trace), we estimated  $\dot{D}_{\max}$  by representing the slip rate as an isosceles triangle of base  $T = 2$  ms and height  $\dot{D}_{\max}$ . The area of the triangle is the slip  $D$ , which can be readily measured and so this triangle representation of slip rate permits the maximum rate to be easily estimated; that is, the maximum slip rate is twice the average rate. As a check on this procedure we observe that for event 9 the maximum slip rate estimated using the triangle representation is 0.093 m/s (Table 1); whereas the maximum rate for this same event seen on the middle trace of Figure 1a is approximately 0.1 m/s.

The experiment reported by Koizumi *et al.* (2004) used a cylindrical granite sample 19.5 mm in diameter, 40 mm high,

and cut at 45 degrees to the core axis. With an initial normal stress of 330 MPa, the yield stress is 180 MPa, and the slip was measured as 0.32 mm with a rise time of 23  $\mu$ s. After making an adjustment for stiffness and for triaxial loading, which amplifies the slip by a factor of 1.5 compared to biaxial loading (see Table 2 and the appendix of McGarr and Fletcher, 2007), the equivalent slip in biaxial loading is 0.21 mm, and the rise time is still 23  $\mu$ s. As for the biaxial experiments, the direct measurement of slip rate for this high-stress experiment was not feasible because of substantial noise (figure 1b of Koizumi *et al.*, 2004); and so we again used an isosceles triangle with an area equal to the slip,  $D = 0.21$  mm, to estimate the maximum slip rate. With this procedure we find that the maximum rate for this high-stress experiment is about 18.3 m/s.

Figure 2 shows  $\dot{D}_{\max}$  as a function of  $\tau_1$  for the 15 biaxial experiments and the high-stress triaxial event. To test our hypothesis that  $\dot{D}_{\max}$  is linearly related to yield stress we assumed the relation  $\dot{D}_{\max} = a\tau_1$  and fit this equation to the point in Figure 2 representing the median biaxial result, event 9 (Table 1), which yields  $\dot{D}_{\max} = 0.0624\tau_1$ , where  $\dot{D}_{\max}$  is in m/s, and  $\tau_1$  is in MPa. This equation is represented by the solid line (Fig. 2), which passes just a little below the high-stress result, despite several orders of magnitude difference in loading stresses. Our simple equation predicts a maximum slip rate of 11.2 m/s for the high-stress event, whereas the experimental estimate, mentioned before, is 18.3 m/s. Thus, the laboratory evidence supports the idea that slip rate is linearly related to yield stress. If this is also true for the seismogenic fault patches that rupture during earthquakes, then estimating radiated energy from an earthquake is fairly straightforward as we show in the next section.

As an aside, we note that there are a number of stress parameters illustrated in Figure 1, including static stress

Table 1  
Laboratory Results (Adapted from table 1 of Lockner and Okubo, 1983)

Event	$\sigma_n$ MPa	$D$ or $\dot{D}_{\max}^*$ Microns or mm/s	$\tau_1$ MPa	$\Delta\sigma$ MPa	$\tau_a$ MPa	$f(v_R)$	$E_R(7)$ J	$E_R(5)$ J
5	1.66	62	0.94	0.20	0.04	0.29	1.98	2.48
6	1.66	70	0.98	0.23	0.01	0.08	0.56	0.87
7	2.21	73	1.21	0.24	0.06	0.33	3.50	3.91
8	2.21	84	1.26	0.28	0.05	0.26	3.36	4.08
9	2.76	93	1.49	0.31	0.08	0.34	5.95	6.53
10	2.76	97	1.53	0.32	0.07	0.30	5.43	6.27
11	3.31	145	1.83	0.48	0.07	0.23	8.12	10.75
12	3.31	128	1.83	0.42	0.10	0.32	10.24	11.65
13	4.41	127	2.34	0.42	0.17	0.45	17.27	16.13
14	4.41	142	2.40	0.47	0.15	0.39	17.04	17.48
15	4.41	119	2.21	0.39	0.09	0.32	8.57	10.07
16	4.41	134	2.27	0.44	0.09	0.29	9.65	11.57
17	4.41	74	2.07	0.24	0.11	0.48	6.51	5.84
18	4.41	105	2.20	0.35	0.12	0.41	10.08	10.04
19	3.45	126	1.98	0.42	0.07	0.25	7.06	8.82

\*Because of our triangle representation of slip rate and the constant rise time of 2 ms, slip in microns is numerically the same as maximum slip rate in mm/s.

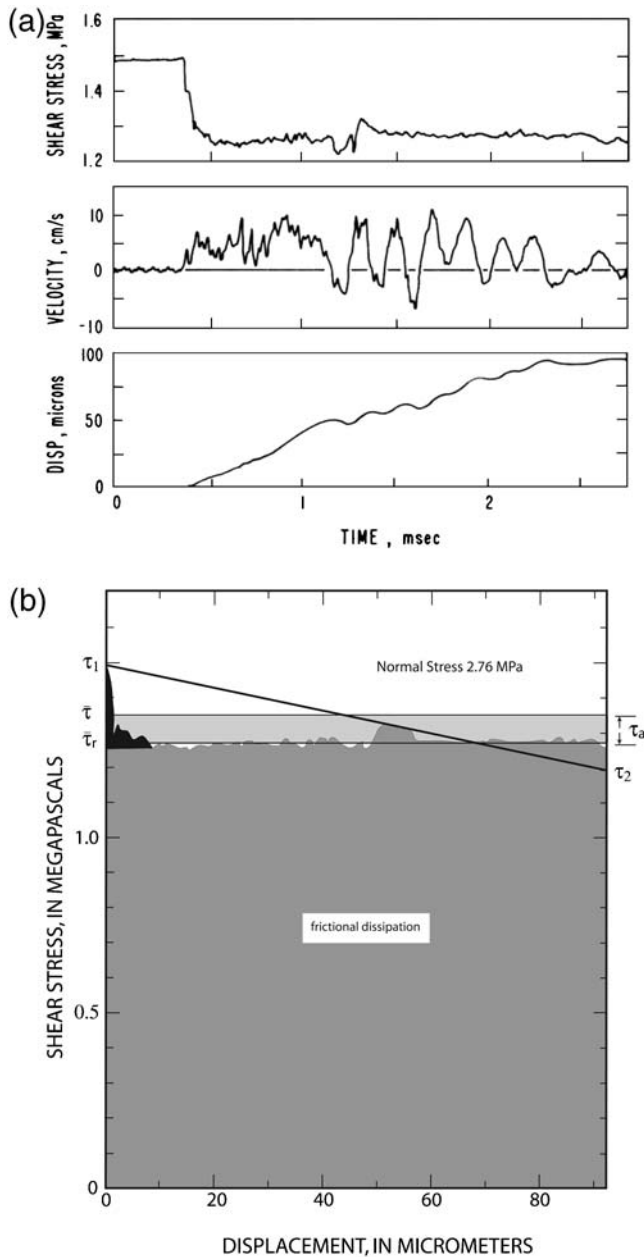


**Figure 1.** (a) Time histories measured for event 9. Top, resisting shear stress; middle, slip rate; bottom, slip. (Originally presented as figure 2 of Lockner and Okubo, 1983.) (b) Various stresses measured for event 9 versus slip. The slope of the heavy line connecting  $\tau_1$  to  $\tau_2$  is the unloading stiffness, 3.3 MPa/mm.  $\bar{\tau}$  is the average loading stress  $\frac{\tau_1 + \tau_2}{2}$ ,  $\bar{\tau}_r$  is the average frictional stress resisting slip, and the apparent stress  $\tau_a = \bar{\tau} - \bar{\tau}_r$  (adapted from figure 4 of Lockner and Okubo, 1983).

drop,  $\Delta\sigma = \tau_1 - \tau_2$ , where  $\tau_2$  is the loading stress at the end of the slip event (Fig. 1b) that are also linearly related to the maximum slip rate (Beeler, 2006). It will be seen in the next section, however, that our analysis requires that we relate slip rate to fault strength in an absolute way. Whereas  $\tau_1$  is an absolute measure of fault strength (Fig. 1b), stress parameters such as  $\Delta\sigma$  indicate stress changes instead of absolute stress or strength.

## Estimating Radiated Energy

We start with a relation developed by McGarr and Fletcher (2001, 2002) for estimating radiated energy  $E_R$  from an earthquake for which a slip model has been developed. Slip models yield the distribution of time-dependent slip  $D(t)$  over the rupture surface from which the near-fault energy flux  $E_{nf}$  from a patch of area  $dA$  can be calculated from  $dE_{nf} = dA\rho\beta \int \dot{D}(t)^2 dt/2$ , where  $\rho$  is the density, and  $\beta$  is the shear wave speed (e.g., Anoushehpour and Brune, 1994). The rupture speed  $v_R$  determines the fraction of this near-fault energy flux  $f(v_R)$  that radiates into the far field. Thus, integrating over the rupture surface gives the seismic energy radiation

$$E_R = \int dA f(v_R) \frac{G}{2\beta} \int \dot{D}(t)^2 dt, \quad (1)$$

where  $G$  is the modulus of rigidity. The dynamic rupture models of Madariaga (1976) and Boatwright (1980) were used by McGarr and Fletcher (2001) to evaluate  $f(v_R)$ , which is 0.11, 0.22, and 0.35 for  $v_R/\beta = 0.6, 0.75$  and 0.9, respectively. As employed by McGarr and Fletcher (2001, 2002), the time integral of equation (1) was evaluated for each subfault comprising the slip model of an earthquake, and then the integral over the fault area was calculated by summing over all of the subfaults.

Here, however, we hypothesize, based on the laboratory evidence (Fig. 2), that the maximum slip rate within a specific subfault depends only on the local yield stress and is independent of any factors specific to the rupture process. For instance, at a given location within the rupture zone,  $\dot{D}_{\max}$  is the same whether the slip in the same patch is 1 mm or 1 m. Similarly, we assert that slip elsewhere in the rupture zone is of no consequence to  $\dot{D}_{\max}$ . As long as any slip occurs within a fault patch that is seismogenic, its maximum slip rate is proportional to the yield stress there.

Using the same procedure as for the laboratory stick-slip events, we parameterize the slip rate within each subfault  $i$  as an isosceles triangle of base  $T_i$ , the time over which the slip increases from zero to  $D_i$ , and of height  $\dot{D}_{\max}^i$ . Thus,

$$D_i = \frac{1}{2} T_i \dot{D}_{\max}^i. \quad (2)$$

With this commonly-used triangle representation of slip rate (e.g., Hartzell and Heaton, 1983), it is easy to find that

$$\int_0^{T_i} \dot{D}_i(t)^2 dt = \frac{1}{3} \dot{D}_{\max}^i{}^2 T_i. \quad (3)$$

Combining (1), (2), and (3) yields for each subfault of area  $A_i$ ,

$$E_R^i = \frac{f^i(v_R)}{3} M_0^i \frac{\dot{D}_{\max}^i}{\beta}, \quad (4)$$

where  $M_0^i$  is the seismic moment of subfault  $i$ . If the product  $f(v_R)\dot{D}_{\max}$  is taken as a slip-weighted average over the rupture zone, then the energy radiated by the earthquake of seismic moment  $M_0$  is given by

Table 2  
Maximum Slips, Maximum Slip Rates, Yield Stresses, and Radiated Energies

Earthquake	$M_0$ N m	$D_{\max}$ m	$v_R/\beta$	$f(v_R)$	$\tau_1$ MPa	$\dot{D}_{\max}$ m/s	$E_R(5)$ J	$E_R(\text{spect})$ J
Adjusted Lab 9, <a href="#">Lockner and Okubo (1983)</a>	4.45e10	5.2e-3		0.34	84.	5.2	8.8e6	8.0e6*
Event 3, <a href="#">McGarr et al. (2009)</a>	4.4e12	27.3e-3		0.34	101.	6.3	8.7e8	1.4e8
Event 4, <a href="#">McGarr et al. (2009)</a>	1.8e12	9.7e-3		0.34	33.	2.0	1.1e8	1.1e8
Event 5, <a href="#">McGarr et al. (2009)</a>	5.4e11	4.3e-3		0.34	18.	1.1	1.9e7	2.3e7
Event 6, <a href="#">McGarr et al. (2009)</a>	4.0e12	9.8e-3		0.34	23.	1.4	1.8e8	6.5e7
12/12/2004	2.3e12	0.025 <a href="#">Reches et al. (2006)</a>		0.34	122.	7.6	5.5e8	5.42e8
12/12/2004	2.3e12	0.016		0.34	62.	3.9	2.8e8	
0310201125, <a href="#">Imanishi and Ellsworth (2006)</a>	1.51e12	14.1e-3		0.34	64.	4.0	2.44e8	2.52e8
Parkfield, <a href="#">Kim and Dreger (2008)</a>	1.3e18	0.45	0.75	0.22	12.	0.77	2.1e13	8.1e13 <a href="#">Baltay et al. (2010)</a>
Parkfield								1.1e13 <a href="#">Ma et al. (2008)</a>
Imperial Valley, <a href="#">Archuleta (1984)</a>	6.7e18	1.55	0.96	0.42	35.	2.2	5.8e14	8.4e14 <sup>†</sup>
Imperial Valley, <a href="#">Hartzell and Heaton (1983)</a>	5.1e18	1.8	0.8	0.25	50.	3.1	3.8e14	
San Simeon, <a href="#">Rolandone et al. (2006)</a>	7.85e18	2.37	0.75	0.22	61.	3.8	6.2e14	9.0e14 <sup>†</sup>
San Simeon, <a href="#">Ji et al. (2004)</a>	6.2e18	2.79	0.9	0.35	88.	5.5	1.1e15	
Northridge, <a href="#">Wald et al. (1996)</a>	1.3e19	2.9	0.83	0.28	64.	4.0	1.3e15	1.2e15 <a href="#">Boatwright et al. (2002)</a> ; <a href="#">Boatwright et al. (unpublished manuscript)</a>
Loma Prieta, <a href="#">Wald et al. (1991)</a>	3.1e19	4.9	0.75	0.22	91.	5.7	3.6e15	4.2e15 <sup>†</sup>
Hector Mine, <a href="#">Kaverina et al. (2002)</a>	6.8e19	5.5	0.68	0.17	73.	4.6	5.2e15	4.5e15 <a href="#">Boatwright et al. (2002)</a> ; <a href="#">Boatwright et al. (unpublished manuscript)</a>
Hector Mine, <a href="#">Ji et al. (2002)</a>	6.28e19	6.9	0.55	0.1	107.	6.9	4.1e15	
Landers, <a href="#">Wald and Heaton (1994)</a>	8.e19	7.9	0.77	0.23	117.	7.3	1.3e16	6.7e15 <sup>†</sup>
Landers, <a href="#">Hernandez et al. (1999)</a>	9.e19	6.8	0.88	0.33	87.	5.4	1.5e16	

\*Estimated using equation (7).

<sup>†</sup>Estimates by J. Boatwright and L. Seekins (personal commun., 2008).

$$E_R(5) = \frac{f(v_R)}{3} M_0 \frac{\dot{D}_{\max}}{\beta}, \quad (5)$$

where we have assumed that all of the slip that contributes to  $M_0$  is due to dynamic rupture. To the extent that aseismic creep adds to the measured  $M_0$ , equation (5) would overestimate the actual radiated energy.

It is worth noting that in deriving equation (5), there is no need to assume that a subfault slips only once. If a subfault slips more than once, then the repeated slip contributes to  $M_0$ , but  $\dot{D}_{\max}$  for that patch is presumably unaffected. Additional slip on subfault  $i$  is the same as adding more  $M_0^i$  in equation (4). That is, whether the time history of slip for a patch is represented as a single triangle or two triangles separated in time makes no difference to the radiated energy as calculated using equation (5).

The key step in the derivation of equation (5) is our assertion, based on laboratory evidence (Fig. 2), that the maximum slip rate is linear in the local yield strength within the rupture zone. This decoupling of  $\dot{D}_{\max}$  from the temporal and spatial distributions of slip leads to considerable simplification in the estimation of radiated energy. In the following

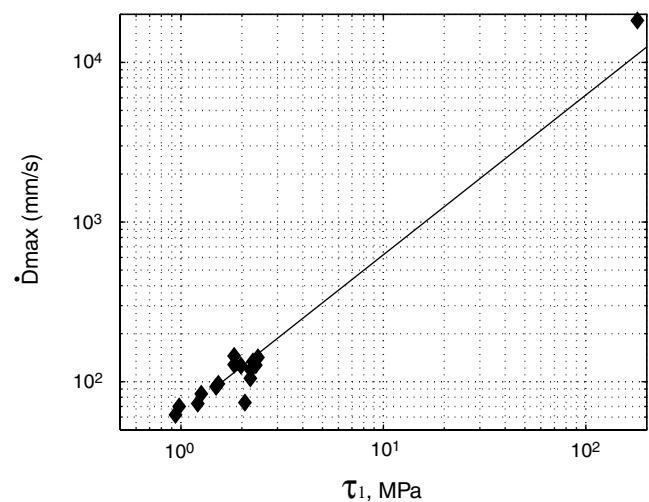


**Figure 2.** Maximum slip rate as a function of yield stress. The sloping line represents a linear relation between maximum slip rate and yield stress fit to event 9 near the lower left corner. (Based on data listed in table 1 of [Lockner and Okubo \[1983\]](#) and the higher-stress experiment reported by [Koizumi et al. \[2004\]](#)).

sections we test this hypothesis by using equation (5) to estimate radiated energies for various types of earthquakes for comparison with independent estimates of this parameter.

### Testing Equation (5) in the Laboratory

Results from biaxial stick-slip experiments reported by Lockner and Okubo (1983) can be used to test equation (5) against more direct measurements of radiated energy from these events. Table 1 lists the slip  $D$ , the static stress drop  $\Delta\sigma$ , and the apparent stress  $\tau_a$  for 15 stick-slip events from table 1 of McGarr (1994), which was adapted from table 1 of Lockner and Okubo (1983). For these laboratory experiments, the static stress drop is the difference between the initial and final loading stresses,  $\tau_1 - \tau_2$ , whereas the apparent stress is the difference between the average loading stress and the average resisting stress (Fig. 1b).  $f(v_R)$ , in equation (5), can be calculated for laboratory stick-slip friction events using (McGarr and Fletcher, 2001)

$$f(v_R) = \frac{\tau_a}{\tau_a + \Delta\sigma/2}. \tag{6}$$

These results are listed in column seven of Table 1. By definition, the apparent stress is the stress that produces radiated energy; that is,  $\tau_a$  is the radiated energy per unit slip per unit fault area. In Figure 1b the lightly-shaded area of average height  $\tau_a$  represents the radiated energy per unit fault area. Thus, the directly measured seismic energy, listed in column eight of Table 1, is given by

$$E_R(7) = AD\tau_a, \tag{7}$$

where  $A$  is the fault area of the biaxial friction experiment.

The results of using equation (5) for the stick-slip experiments are listed in column nine of Table 1; in evaluating equations (5) and (7),  $M_0 = GAD$ ,  $G = 2.5 \times 10^{10}$  Pa,  $A = 0.8 \text{ m}^2$  ( $2 \times 0.4 \text{ m}$ ) and  $\beta = 3000 \text{ m/s}$  (Lockner and Okubo, 1983); both  $D$  and  $\dot{D}_{\text{max}}$  are listed in column three of Table 1.

The energies listed in the last two columns of Table 1 are plotted against each other in Figure 3 where we see that the estimates based on equations (7) and (5) are in good agreement. All of the points lie close to the line representing  $E_R(5) = E_R(7)$ . Although there is a small tendency for  $E_R(5)$  to be greater than  $E_R(7)$ , these laboratory results, nonetheless, indicate that equation (5) is an effective way to estimate radiated energy.

To find out whether equation (5) works for earthquakes, the main challenge is to determine maximum slip rates. The next section reviews a procedure for doing this.

### Maximum Slip Rates for Earthquakes

To estimate the maximum slip rate for an earthquake source, we match the laboratory stick-slip experiments to an earthquake using a procedure described by McGarr *et al.*

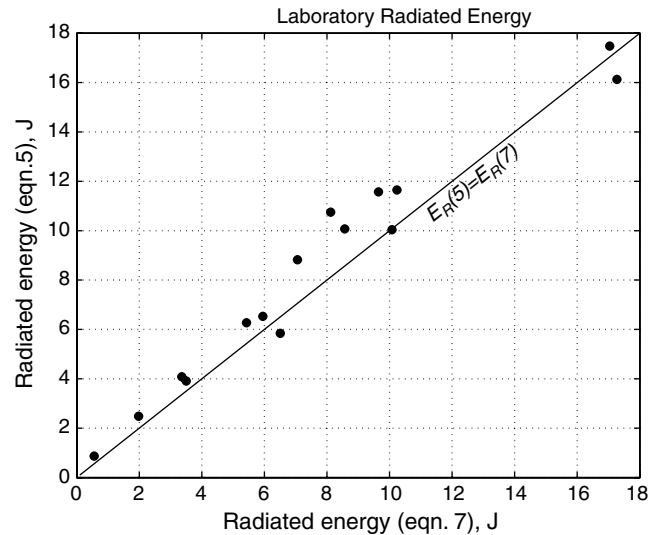


**Figure 3.** Radiated energy for stick-slip friction events calculated using equation (5) as a function of  $E_R$  estimated directly using equation (7).

(2009). The first step of the procedure is to replace the laboratory fault with an equivalent-stiffness buried shear crack. In the second step, we simulate a change in the loading stresses by adjusting the slip of the laboratory experiment until its stress parameters match those of the earthquake. We now review the details of this procedure.

Figure 4 shows maximum slip  $D_{\text{max}}$  within the rupture zone of an earthquake as a function of  $M_0$  and the regression fit, obtained by McGarr and Fletcher (2003), indicating that  $D_{\text{max}}$  scales as the cube root of the seismic moment. Figure 4 also illustrates how we relate laboratory experiments to earthquakes for purposes of estimating maximum slip rates. Of the 15 stick-slip experiments listed in Table 1, event 9 yielded the median maximum slip rate if all the experiments are adjusted for the same normal stress (McGarr *et al.*, 2009).

We now describe the steps in adjusting event 9 analytically so as to match the stress parameters of an earthquake. The triangle marked L&O(1) in Figure 4 represents the raw experimental result,  $D = 93 \times 10^{-6} \text{ m}$ ,  $M_0 = 1.86 \times 10^6 \text{ N m}$  (Fig. 1, Table 1). The first step is to replace its actual fault surface (2 m by 0.4 m) with that of a buried penny-shaped shear crack that has the same stiffness (Walsh, 1971). This stiffness is given by  $k = \frac{\Delta\sigma}{D} = \frac{7\pi G}{16r}$ , where  $D$  is the average slip, and  $r$  is the radius of the crack (Eshelby, 1957; Keilis-Borok, 1959). To simulate the laboratory stiffness of 3.3 MPa/mm, we set  $r = 10.4 \text{ m}$ . The triangle marked L&O(2) in Figure 4 represents event 9 after the stiffness adjustment. Thus, the stiffness-adjusted event 9 has its original slip of  $93 \times 10^{-6} \text{ m}$  (Table 1) but is much larger in area, with a seismic moment of  $7.9 \times 10^8 \text{ N m}$  because the stiffness is the same as for the laboratory setup; the rise time for the slip is still 2 ms.

To illustrate the second step of our procedure, we will adjust event 9 so as to determine the slip rate for earthquakes that plot on the regression line in Figure 4. All of the experi-

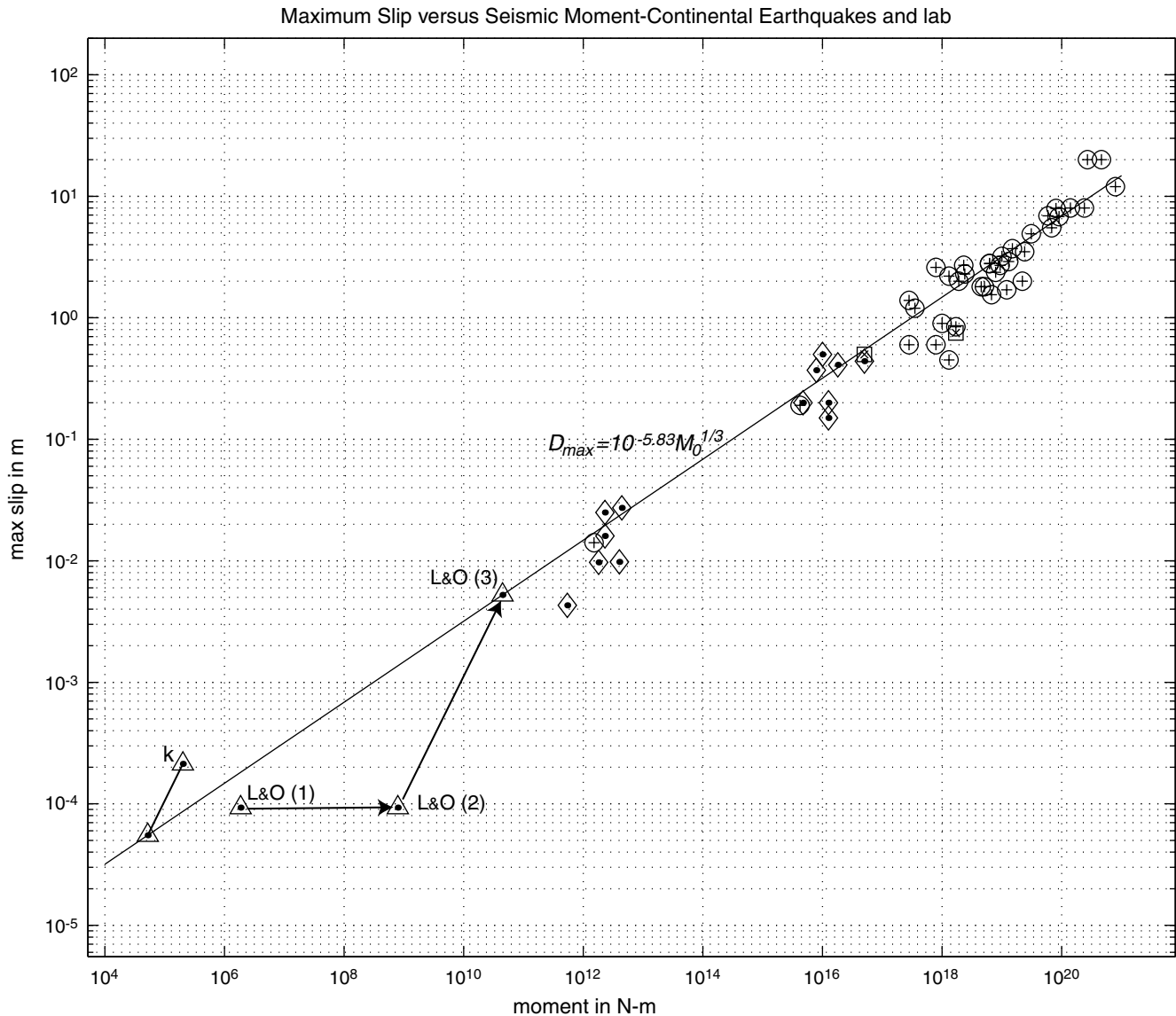


**Figure 4.** Maximum slip within rupture zones of earthquakes in continental settings as functions of seismic moment (adapted from figure 2 of McGarr and Fletcher, 2003). The points near  $M_0 = 10^{12}$  N m were reported by McGarr *et al.* (2009) (see Table 2). The triangles represent laboratory results. The arrow between L&O(1) and L&O(2) illustrates the stiffness adjustment for event 9 (Table 1) and the arrow between L&O(2) and L&O(3) shows the loading stress adjustment. The triangle marked  $k$  represents the experiment by Koizumi *et al.* (2004) after a stiffness adjustment and the line extending downward and leftward shows the stress adjustment needed to match the stresses and slip rate of the regression line (see text).

ments of Lockner and Okubo (1983) were conducted using a deformation apparatus of constant unloading stiffness on a sample of constant fault area, and so the only way to produce an event with larger slip or seismic moment would be to increase the loading stresses. This implies a linear relation between loading stress and slip and so, to simulate an increase in loading stress, we increase the slip  $D$  analytically until the adjusted version of event 9 falls on the regression line. The adjusted slip  $D_{ad}$  is determined by solving

$$D_{ad} = C(\pi r^2 G D_{ad})^{1/3}, \quad (8)$$

where  $r = 10.4$  m,  $G = 2.5 \times 10^{10}$  Pa, and  $C = 10^{-5.83}$  for the regression line (Fig. 4). The solution is  $D_{ad} = 5.2$  mm.

The solid line connecting triangle L&O(2) to L&O(3) illustrates this second adjustment. Because the rise time is unaffected by the loading stresses, it is still 2 ms. Thus, as the maximum slip rate is twice the average, the adjusted maximum slip rate is 5.2 m/s.

Although we effected the second adjustment of event 9 by simply increasing the slip, to replicate this result experimentally, we would increase the loading stresses by the ratio  $D_{ad}/D = 56$ . Accordingly, the analytically-adjusted experiment involves loading stresses and stress changes that are 56 times greater than those for event 9. Any point along the regression line in Figure 4 has the same slip rate (5.2 m/s) and loading stresses ( $\tau_1 = 84$  MPa) as those listed in Table 2

for the adjusted version of laboratory event 9. We also note that our choice of event 9, among the experiments listed in Table 1, is immaterial to the maximum slip rate result. Any of the experiments would have given the same maximum slip rate of 5.2 m/s because all of the experiments in Table 1, if plotted in Figure 4, would fall on the line connecting the triangle marked L&O(2) to the one marked L&O(3) on the regression line. The adjusted yield stresses for these experiments (Table 1), in contrast, vary from 66 MPa for event 11 up to 147 MPa for event 17; the median yield stress is 84 MPa, as listed in Table 2 for event 9.

Thus, our procedure for estimating slip rate and stress information for any of the earthquakes for which we know the seismic moment and the maximum slip within the rupture zone is to determine  $C$  in the expression

$$D_{\max} = CM_0^{1/3} \quad (9)$$

for a particular earthquake. Once  $C$  is evaluated, we follow the steps just described to estimate the maximum slip rate and the yield stress, as well as any other stress parameters of interest.

This procedure for estimating the maximum slip rates relies on the 15 experiments listed in Table 1. To get some idea about how robust these biaxial laboratory results, run at low loading stresses, are for the purpose of estimating maximum slip rate within an earthquake source, we again consider the experiment reported by Koizumi *et al.* (2004). Whereas the biaxial friction experiments listed in Table 1 were run at normal stresses ranging up to 4.4 MPa, the test described by Koizumi *et al.* (2004) was performed at an initial normal stress of 330 MPa (see table 2 of McGarr and Fletcher, 2007) applied to a pre-cut fault through a small sample in triaxial loading conditions. As described previously, for this high-stress stick-slip event, the corrected slip is 0.21 mm and the rise time is 23  $\mu$ s. The radius of the buried circular crack with the same unloading stiffness as the laboratory test is 0.1 m (see table 2 of McGarr and Fletcher, 2007). Assuming that the granite sample has a modulus of rigidity of  $3 \times 10^4$  MPa, then the seismic moment is  $2.0 \times 10^5$  N m.

We see in Figure 4 (lower left-hand corner) that the triangle marked  $k$ , representing the experimental result of Koizumi *et al.* (2004), adjusted for stiffness as just described, plots above the regression line through the earthquake data, suggesting that the loading stresses for this experiment are higher than those typically causing earthquakes at seismogenic depths. If we follow the same procedure as before and adjust the Koizumi *et al.* (2004) result so that it falls on the regression line, then from equations (8) and (9), the slip is adjusted from  $2.1 \times 10^{-4}$  m down to  $5.5 \times 10^{-5}$  m, with an adjusted seismic moment of  $5.2 \times 10^4$  N m, along the line shown in Figure 4. Because the rise time is still 23  $\mu$ s, the adjusted maximum slip rate is 4.8 m/s, which is only slightly less than the rate derived from the biaxial experiments listed in Table 1. Thus, after accounting for the loading stresses, as

illustrated in Figure 4, the results from Koizumi *et al.* (2004) appear to be consistent with those from the biaxial friction experiments in terms of the inferred maximum slip rate at seismogenic depths.

Although the agreement between the high-stress experiment reported by Koizumi *et al.* (2004) and the lower-stress biaxial events (Table 1) is encouraging, we have, nonetheless, considered only the biaxial results in the following analysis, mostly because these experiments are thought to replicate earthquakes better than their triaxial counterparts and also because there are 15 of them instead of only one. Thus, the maximum slip rate for points that plot on the regression line in Figure 4 is still taken to be 5.2 m/s for purposes of our analysis.

### Testing Equation (5) Using Earthquake Data

To test the viability of our approach, we analyzed 13 earthquakes for which radiated energy has been estimated independently, mostly from spectra of ground velocity. In addition to adjusted laboratory event 9, Table 2 lists six small earthquakes with magnitudes near 2 that were reported by McGarr *et al.* (2009) and seven major, well-studied, earthquakes in California.

Of the six small earthquakes, events 3 to 6 and 12 December 2004 (Table 2) were induced by deep mining operations in South Africa (McGarr *et al.*, 2009) and event 0310201125 was located within a cluster of repeating earthquakes on the San Andreas fault near the San Andreas Fault Observatory at Depth (SAFOD) site, California (Imanishi and Ellsworth, 2006). The seismic moments of the five mining-induced earthquakes are the deviatoric components of the moment tensors calculated by M. Boettcher *et al.* (unpublished manuscript; see also Boettcher *et al.*, 2009), using an updated version of a method reported by McGarr (1992), and for event 0310201125,  $M_0$  is from Table 1 of Imanishi and Ellsworth (2006).

As described by McGarr *et al.* (2009), maximum slips for these six earthquakes were estimated using

$$R\bar{v} = 0.087\beta D_{\max}, \quad (10)$$

where  $R$  is the hypocentral distance and  $\bar{v}$  is the  $Q$ -corrected, vectorially summed peak ground velocity (Table 2 and Fig. 4). Equation (10), developed by McGarr *et al.* (2009), has some model dependence, and so, as described by those authors, it has been tested against underground observations of slip across exhumed ruptures associated with recorded mining-induced earthquakes and found to be effective. In the case of event 12 December 2004, for example, a maximum slip of 25 mm was measured underground in the rupture zone (Reches *et al.*, 2006), whereas that estimated from the peak velocity is 16 mm (McGarr *et al.*, 2009); there is uncertainty associated with each estimate of  $D_{\max}$  and so both are listed in Table 2 and analyzed here. There are no rupture speed estimates for these small earthquakes, and so we have

assumed that  $f(v_R) = 0.34$ , the result for laboratory event 9. This corresponds to a rupture speed slightly less than  $0.9\beta$ .

Slip models developed for the seven California earthquakes yielded the estimates of  $M_0$ ,  $D_{\max}$ , and  $v_R$  listed in Table 2;  $v_R$  is taken here as the average rupture speed over the fault zone for a particular slip model. For four of these earthquakes, we have listed two independent slip models to provide an indication of the uncertainty associated with choice of slip model.

The next step is to follow the procedure outlined in the preceding section to estimate the maximum slip rate by first determining  $C$  for each  $(M_0, D_{\max})$  pair using equation (9), then solving equation (8) for the adjusted laboratory slip  $D_{\text{ad}}$ , and finally converting  $D_{\text{ad}}$  to a maximum slip rate based on a constant rise time of 2 ms. As seen in Table 2, the resulting maximum slip rates vary from 0.8 m/s for the 2004 Parkfield, California, earthquake (Kim and Dreger, 2008), up to 7.3 m/s based on the slip model developed for the 1992 Landers, California, earthquake by Wald and Heaton (1994).

The yield stresses,  $\tau_1$ , listed in Table 2, were estimated by multiplying the yield stress of event 9, 1.49 MPa (Table 1), by  $D_{\text{ad}}/D$ , where  $D = 93$  microns. As analyzed here, these yield stresses are proportional to the corresponding maximum slip rates (Fig. 2). If the yield stresses are taken at face

value, then there appears to be quite a substantial variation in fault-zone strength among the earthquakes considered here, a point to which we will return.

The last two columns in Table 2 list the estimates of radiated energy based on equation (5) and on the spectra of ground velocity,  $E_R(5)$  and  $E_R(\text{spect})$ , respectively. Figure 5 shows these results for the six small earthquakes. M. Boettcher *et al.* (unpublished manuscript) estimated the radiated energies  $E_R(\text{spect})$  (Table 2) for the five mining-induced earthquakes from  $Q$ -corrected spectra of the ground velocities recorded by the broadband stations installed at depths between 2 km and 3.6 km within two deep gold mines (McGarr *et al.*, 2009). For event 0310201125, the repeater near the SAFOD site,  $E_R(\text{spect})$  was estimated from ground-motion data recorded in the SAFOD pilot hole by Imanishi and Ellsworth (2006). Of the six small earthquakes (Fig. 5 and Table 2) the two different estimates of  $E_R$  are all in good agreement except event 3, for which there is a factor of 6 discrepancy.

Similar results for seven major earthquakes in California are shown in Figure 6 and listed in Table 2. For six of these earthquakes, Boatwright and his colleagues (e.g., Boatwright *et al.*, 2002; unpublished manuscript) have used extensive sets of regional ground-motion data to determine radiated energies, all estimated using the same method. Their energy

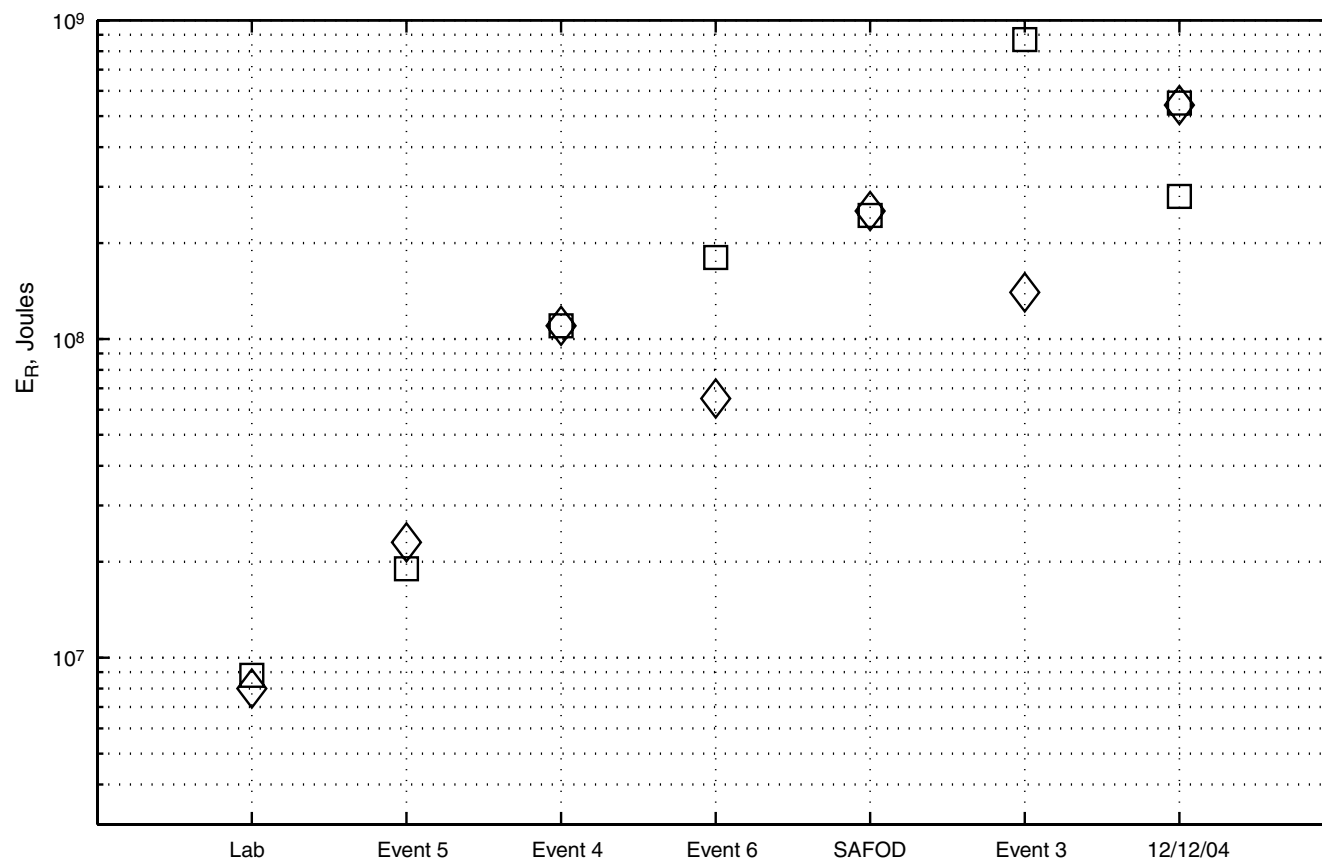


**Figure 5.** Radiated energies for the small earthquakes and the adjusted version of laboratory event 9. Diamonds represent spectral estimates and squares are the results of using equation (5). For the lab event, the diamond shows the result based on the direct measurement of the apparent stress, equation (7).

estimates are derived from acceleration spectra of  $S$ ,  $Lg$  and surface waves over the frequency band 0.05 to 20 Hz. In the case of the 2004 Parkfield earthquake, we have listed two independent estimates of  $E_R$  (Table 2) for comparison with the estimate from equation (5). The estimate by [Baltay et al. \(2010\)](#),  $8.1 \times 10^{23}$  J, was made by applying an empirical Green's function method to seismic coda, whereas that by [Ma et al. \(2008\)](#),  $1.1 \times 10^{13}$  J, is from their preferred dynamic rupture model. For these California earthquakes the agreement between the spectral estimates of  $E_R$  and the estimates using equation (5) is reasonably good (Table 2, Fig. 6).

Figure 7 plots all of the energies listed in Table 2 as functions of seismic moment. The solid line indicates a constant apparent stress of 3.5 MPa. This line is not a regression fit to these data, but it, nonetheless, provides a good fit, indicating that the ratio of energy to moment shows no systematic variation with  $M_0$ .

### Discussion

As demonstrated in Table 2, equation (5) seems to be remarkably effective for estimating  $E_R$ , especially considering its simplicity, which derives from the idea that there exists a slip-averaged maximum slip rate that is controlled by the strength of the seismogenic zone. Whereas the distribution of slip within the rupture zone of an earthquake can be quite heterogeneous and unpredictable from one earthquake to the next, the slip rate shows much simpler behavior in that it appears to be linearly related to the seismogenic strength. This aspect of slip rate renders the estimation of radiated energy much easier than if the slip rate at a given point were influenced by the distribution of slip within the rupture zone or some other factor specific to a particular earthquake rupture.

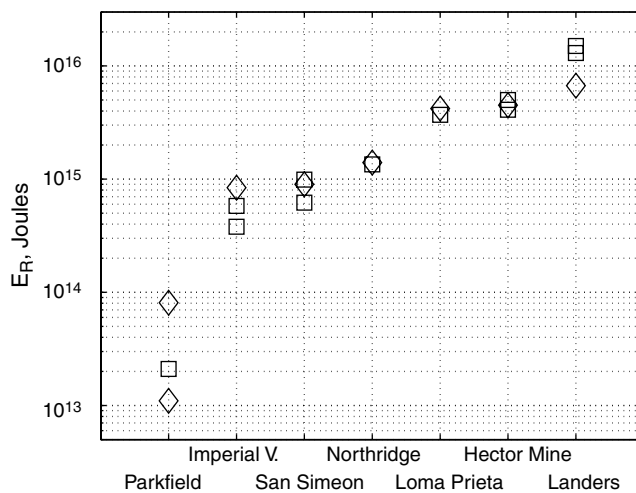


**Figure 6.** Radiated energies for seven major earthquakes in California. The diamonds represent estimates based on spectra of ground motion at local and regional distances and the squares show results of applying equation (5) to slip model parameters,  $M_0$ ,  $D_{max}$ , and  $v_R$ .

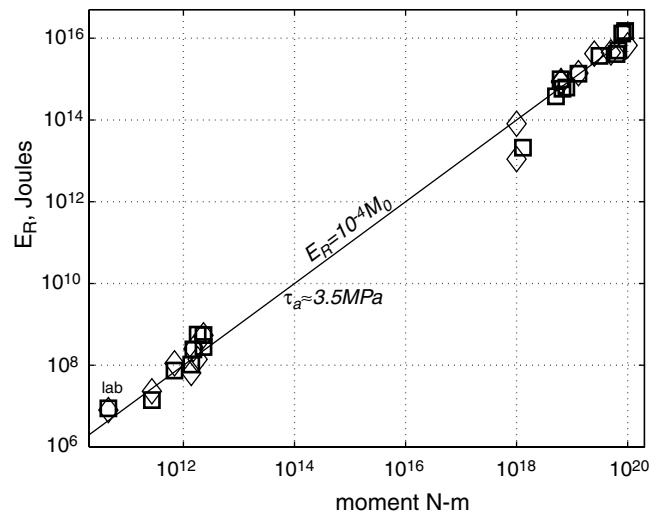


**Figure 7.** Radiated energies vs.  $M_0$  for all of the earthquakes and slip models listed in Table 2. Diamonds indicate spectral estimates and squares indicate results from using equation (5); for the lab event, the diamond shows the result of using equation (7).

Laboratory friction results play an important role in our analysis in that they allow an estimate of the maximum slip rate for any earthquake for which both the seismic moment and the maximum slip have been estimated. By adjusting the loading stresses analytically so as to fit a laboratory experiment to a particular earthquake, we are able to estimate the maximum slip rate, as illustrated in Figure 4, as well as the yield stress in the seismogenic zone where the maximum slip occurs. The maximum slip rates obtained here (Table 2) appear to be credible inasmuch as they largely agree with slip rates obtained using an entirely different procedure by [McGarr and Fletcher \(2007\)](#). Moreover, as just demonstrated, these maximum slip rates yield credible estimates of radiated energy.

Are the yield stresses resulting from the same analysis (Table 2) also realistic? To address this question, we consider typical yield stresses of the earthquakes listed in Table 2 and, separately, the exceptionally low yield stress found for the 2004  $M$  6 Parkfield earthquake. For all of the earthquake yield stresses listed in Table 2, the median is  $\tau_1 = 64$  MPa. If we just consider the results for the major earthquakes in California (Table 2), the median is  $\tau_1 = 73$  MPa. Both of these medians are reasonably close to the shear stress  $\tau$ , resolved on the optimum plane of shear failure measured at a depth of 6.8 km in the KTB scientific borehole in Germany ([Brudy et al., 1997](#); [McGarr and Fletcher, 2003](#)),  $\tau = 65$  MPa. Thus, the yield stresses inferred here (Table 2) appear to be more or less consistent with the deepest measured *in situ* stresses.

The yield stress for the 2004 Parkfield earthquake of 12 MPa, in contrast, is much lower. Our estimate of  $\tau_1$  is based on the slip model of [Kim and Dreger \(2008\)](#). Other slip models that have been developed for this earthquake, although based on different data sets, would have resulted in similarly low estimates of the yield stress inasmuch as they

all have maximum slips that are low for  $M$  6 earthquakes (McGarr and Fletcher, 2003). For the preferred model of Liu *et al.* (2006), for example, the maximum slip is 0.57 m, and the yield stress would have been 19 MPa. Accordingly, the low yield stress inferred here for the Parkfield earthquake does not appear to be an artifact of the choice of slip model.

Indeed, a yield stress for the Parkfield earthquake of less than 20 MPa is consistent with other evidence based on heat flow (Williams *et al.*, 2004) and *in situ* stress measurements (Hickman and Zoback, 2004) that suggest that the San Andreas fault near Parkfield has a shear strength of about 20 MPa, or less. This low inferred strength is difficult to understand, but it may be related somehow to the mature nature of the San Andreas fault, a characteristic that often seems to give rise to low apparent stresses (e.g., Choy *et al.*, 2006). The higher yield stress inferred for event 0310201125 of 64 MPa, however, indicates that there are at least some patches of the fault zone in the vicinity of Parkfield that have more typical seismogenic strength.

In a cautionary vein, we note that because our estimate of  $E_R$  for the 2004 Parkfield earthquake from equation (5) is nearly four times smaller than that of Baltay *et al.* (2010) (Table 2), it is perhaps most realistic to regard our inferences concerning this section of the San Andreas fault as tentative. That is, the estimate of Baltay *et al.* (2010) for the energy radiated by the Parkfield earthquake is compatible neither with our estimate of  $E_R$  nor with our low inferred yield stress.

The yield stresses for the mining-induced earthquakes listed in Table 2 show considerable variability, but this is perhaps not surprising considering their seismogenic circumstances. That is, these earthquakes occur within a rock mass for which the state of stress and hydrologic regime have been substantially perturbed from the ambient conditions. The mining operations result in a reduction in pore pressure from approximately hydrostatic to zero and the ore production entails extensive tabular excavations that create localized zones of high stress that lead to seismic rupture of the dry rock mass (McGarr *et al.*, 2009).

Needless to say, the results listed in Table 2 have uncertainty and the main source is probably uncertainty in  $D_{\max}$ . The two different estimates of  $D_{\max}$  for event 12 December 2004 allow us to assess the effect of uncertainty in  $D_{\max}$  on the maximum slip rate and the stress parameters. From Table 2, we see that whereas the higher slip, 25 mm, is a factor of 1.56 greater than the lower estimate, 16 mm, the corresponding difference in inferred maximum slip rates, yield stress, and radiated energy, is a factor of about 1.96. Thus, it seems that error in  $D_{\max}$  leads to somewhat greater errors in the inferred estimates of  $\dot{D}_{\max}$ ,  $\tau_1$ , and  $E_R$  (5).

## Conclusions

In brief summary, our main conclusions are

1. The results of laboratory stick-slip friction experiments support the hypothesis that maximum slip rates within earthquake rupture zones depend linearly on seismogenic strength.
2. The existence of a maximum slip rate that depends only on seismogenic strength leads to equation (5), a straightforward relationship for radiated energy based on the seismic moment, the maximum slip rate and the rupture speed.
3. After testing equation (5) using laboratory stick-slip events, we applied it to 13 earthquakes and found that it yields radiated energies that agree, for the most part, with independent estimates based on spectra of ground velocity recorded at local and regional distances.
4. Fitting the laboratory friction results to a given earthquake also gives stress parameters, including the yield stress.
5. On the one hand, the yield stresses obtained for the earthquakes of our study, typically in the range 35 to 90 MPa, are consistent with the deepest available *in situ* stress measurements, but, on the other hand, the 2004 Parkfield  $M$  6 earthquake shows a yield stress inferred, at least tentatively, to be less than 20 MPa, consistent with other local indicators of low fault-zone strength including heat flow and *in situ* stress measurements.

## Data and Resources

The IRIS/PASSCAL ground-motion data have been archived at the IRIS Data Management Center (DMC). Users of these data can register through the Internet at [http://www.iris.edu/data/restricted\\_req.htm](http://www.iris.edu/data/restricted_req.htm). The borehole seismic data from the SAFOD Pilot Hole are archived at the Northern California Earthquake Data Center. Data for earthquakes near SAFOD can be accessed at <http://www.ncedc.org/2004parkfield.html>. The in-mine network data used here are proprietary.

## Acknowledgments

We thank George Choy and Tom Hanks for insightful reviews of an earlier version of this manuscript. We are grateful to Chris Marone for very comprehensive review comments that were quite helpful.

## References

- Anooshehpour, A., and J. N. Brune (1994). Frictional heat generation and seismic radiation in a foam rubber model of earthquakes, *Pure Appl. Geophys.* **142**, 735–747.
- Archuleta, R. J. (1984). A faulting model for the 1979 Imperial Valley earthquake, *J. Geophys. Res.* **89**, 4559–4585.
- Baltay, A. S., G. A. Prieto, and G. C. Beroza (2010). Radiated seismic energy from coda measurements and no scaling in apparent stress with seismic moment, *J. Geophys. Res.* **115**, B08314, doi [10.1029/2009JB006736](https://doi.org/10.1029/2009JB006736).
- Beeler, N. M. (2006). Inferring earthquake source properties from laboratory observations and the scope of lab contributions to source physics, in *Earthquakes: Radiated Energy and the Physics of Faulting*, R. Abercrombie, A. McGarr, H. Kanamori, and G. Di Toro (Editors), AGU Geophysical Monograph Series 170, 99–119.

- Boatwright, J. (1980). A spectral theory for circular seismic sources: simple estimates of source dimension, dynamic stress drop, and radiated seismic energy, *Bull. Seismol. Soc. Am.* **70**, 1–27.
- Boatwright, J., G. L. Choy, and L. C. Seekins (2002). Regional estimates of radiated energy, *Bull. Seismol. Soc. Am.* **92**, 1241–1255.
- Boettcher, M. S., A. McGarr, and M. Johnston (2009). Extension of Gutenberg-Richter distribution to  $M_w$ -1.3, no lower limit in sight, *Geophys. Res. Lett.* **36**, L10307, doi [10.1029/2009GL038080](https://doi.org/10.1029/2009GL038080).
- Brace, W. F., and J. D. Byerlee (1966). Stick slip as a mechanism for earthquakes, *Science* **153**, 990–992.
- Brudy, M., M. D. Zoback, K. Fuchs, F. Rummel, and J. Baumgartner (1997). Estimation of the complete stress tensor to 8 km depth in the KTB scientific drill holes: implications for crustal strength, *J. Geophys. Res.* **102**, 18,453–18,475.
- Byerlee, J. D. (1968). Brittle-ductile transition in rocks, *J. Geophys. Res.* **73**, 4741–4750.
- Choy, G. L., A. McGarr, S. H. Kirby, and J. Boatwright (2006). An overview of the global variability in radiated energy and apparent stress, in *Earthquakes: Radiated Energy and the Physics of Faulting*, R. Abercrombie, A. McGarr, H. Kanamori, and G. Di Toro (Editors), AGU Geophysical Monograph Series 170, 43–57.
- Dieterich, J. H. (1981). Potential for geophysical experiments in large-scale tests, *Geophys. Res. Lett.* **8**, 653–656.
- Eshelby, J. (1957). The determination of the elastic field of an ellipsoidal inclusion and related problems, *Proc. R. Soc. London Ser. A* **241**, 376–396.
- Hartzell, S. H., and T. H. Heaton (1983). Inversion of strong ground motion and teleseismic waveform data for the fault rupture history of the 1979 Imperial Valley, California, earthquake, *Bull. Seismol. Soc. Am.* **73**, 1553–1583.
- Hernandez, B., F. Cotton, and M. Campillo (1999). Contribution of radar interferometry to a two-step inversion of the kinematic process of the 1992 Landers earthquake, *J. Geophys. Res.* **104**, 13,083–13,099.
- Hickman, S., and M. D. Zoback (2004). Stress orientations and magnitudes in the SAFOD pilot hole, *Geophys. Res. Lett.* **31**, L15S12, doi [10.1029/2004GL020043](https://doi.org/10.1029/2004GL020043).
- Imanishi, K., and W. L. Ellsworth (2006). Source scaling relationships of microearthquakes at Parkfield, CA, determined using the SAFOD pilot hole seismic array, in *Earthquakes: Radiated Energy and the Physics of Faulting*, R. Abercrombie, A. McGarr, H. Kanamori, and G. Di Toro (Editors), AGU Geophysical Monograph Series 170, 81–90.
- Ji, C., K. M. Larsen, Y. Tan, K. W. Hudnut, and K. Choi (2004). Slip history of the 2003 San Simeon earthquake constrained by combining 1-Hz GPS, strong motion, and teleseismic data, *Geophys. Res. Lett.* **31**, L17608, doi [10.1029/2004GL020448](https://doi.org/10.1029/2004GL020448).
- Ji, C., D. J. Wald, and D. V. Helmberger (2002). Source description of the 1999 Hector Mine, California, earthquake, Part II: Complexity of slip history, *Bull. Seismol. Soc. Am.* **92**, 1208–1226.
- Johnson, T., and C. Scholz (1976). Dynamic properties of stick-slip friction of rock, *J. Geophys. Res.* **81**, 881–888.
- Kaverina, A., D. Dreger, and E. Price (2002). The combined inversion of seismic and geodetic data for the source process of the 16 October 1999  $M_w$  7.1 Hector Mine, California, earthquake, *Bull. Seismol. Soc. Am.* **92**, 1266–1280.
- Keilis-Borok, V. I. (1959). On estimation of the displacement in an earthquake source and of source dimensions, *Ann. Geofis.* **12**, 205–214.
- Kim, A., and D. S. Dreger (2008). Rupture process of the 2004 Parkfield earthquake from near-fault seismic waveform and geodetic records, *J. Geophys. Res.* **113**, B07308, doi [10.1029/2007JB005115](https://doi.org/10.1029/2007JB005115).
- Koizumi, Y., K. Otsuki, A. Takeuchi, and H. Nagahama (2004). Frictional melting can terminate seismic slips: experimental results of stick-slips, *Geophys. Res. Lett.* **31**, L21065, doi [10.1029/2004GL020642](https://doi.org/10.1029/2004GL020642).
- Liu, P., S. Custodio, and R. J. Archuleta (2006). Kinematic inversion of the 2004  $M_w$  6.0 Parkfield earthquake including site effects, *Bull. Seismol. Soc. Am.* **96**, S143–S158.
- Lockner, D. A., and P. G. Okubo (1983). Measurements of frictional heating in granite, *J. Geophys. Res.* **88**, 4313–4320.
- Ma, S., S. Custodio, R. J. Archuleta, and P. Liu (2008). Dynamic modeling of the 2004  $M_w$  6.0 Parkfield, California, earthquake, *J. Geophys. Res.* **113**, B02301, doi [10.1029/2007JB005216](https://doi.org/10.1029/2007JB005216).
- Madariaga, R. (1976). Dynamics of an expanding circular fault, *Bull. Seism. Soc. Am.* **66**, 639–666.
- McGarr, A. (1992). An implosive component in the seismic moment tensor of a mining-induced tremor, *Geophys. Res. Lett.* **19**, 1579–1582.
- McGarr, A. (1994). Some comparisons between mining-induced and laboratory earthquakes, *Pure Appl. Geophys.* **142**, 467–489.
- McGarr, A., and J. B. Fletcher (2001). A method for mapping apparent stress and energy radiation applied to the 1994 Northridge earthquake fault zone—revisited, *Geophys. Res. Lett.* **28**, 3529–3532.
- McGarr, A., and J. B. Fletcher (2002). Mapping apparent stress and energy radiation over the fault zones of major earthquakes, *Bull. Seismol. Soc. Am.* **92**, 1633–1644.
- McGarr, A., and J. B. Fletcher (2003). Maximum slip in earthquake fault zones, apparent stress, and stick-slip friction, *Bull. Seismol. Soc. Am.* **93**, 2355–2362.
- McGarr, A., and J. B. Fletcher (2007). Near-fault peak ground velocity from earthquake and laboratory data, *Bull. Seismol. Soc. Am.* **97**, 1502–1510.
- McGarr, A., M. Boettcher, J. B. Fletcher, R. Sell, M. J. S. Johnston, R. Durrheim, S. Spottiswoode, and A. Milev (2009). Broadband records of earthquakes in deep gold mines and a comparison with results from SAFOD, California, *Bull. Seismol. Soc. Am.* **99**, 2815–2824.
- Reches, Z., and Drilling Active Faults in South African Mines and the Natural Earthquake Laboratory in South African Mines Teams (2006). Building a natural earthquake laboratory at focal depth (DAFSAM-NELSAM Project, South Africa), *Sci. Drilling* doi [10.2204/iodp.sd.3.06.2006](https://doi.org/10.2204/iodp.sd.3.06.2006), 30–33.
- Rolandone, F., D. Dreger, M. Murray, and R. Burgmann (2006). Coseismic slip distribution of the 2003  $M_w$  6.6 San Simeon earthquake, California, determined from GPS measurements and seismic waveform data, *Geophys. Res. Lett.* **33**, L16315, doi [10.1029/2006GL027079](https://doi.org/10.1029/2006GL027079).
- Wald, D. J., and T. H. Heaton (1994). Spatial and temporal distribution of slip for the 1992 Landers, California, earthquake, *Bull. Seismol. Soc. Am.* **84**, 668–691.
- Wald, D. J., T. H. Heaton, and D. V. Helmberger (1991). Rupture model of the 1989 Loma Prieta earthquake from the inversion of strong motion and broadband teleseismic data, *Bull. Seismol. Soc. Am.* **81**, 1540–1572.
- Wald, D. J., T. H. Heaton, and K. W. Hudnut (1996). The slip history of the 1994 Northridge, California, earthquake determined from strong motion, teleseismic, GPS, and leveling data, *Bull. Seismol. Soc. Am.* **86**, S49–S70.
- Walsh, J. B. (1971). Stiffness in faulting and friction experiments, *J. Geophys. Res.* **76**, 8597–8598.
- Williams, C. F., F. V. Grubb, and S. P. Galanis (2004). Heat flow in the SAFOD pilot hole and implications for the strength of the San Andreas fault, *Geophys. Res. Lett.* **31**, L15S14, doi [10.1029/2003GL019352](https://doi.org/10.1029/2003GL019352).
- U.S. Geological Survey  
MS 977, 345 Middlefield Rd.  
Menlo Park, California 94025  
mcgarr@usgs.gov  
(A.M., J.B.F., N.B., J.B.)
- Department of Earth Sciences  
University of New Hampshire  
Durham, New Hampshire 03824  
(M.B.)